Room Temperature Electrodeposition of Molybdenum Sulfide for Catalytic and Photoluminescence Applications

Sankaran Murugesan, Arunkumar Akkineni, Brendan P. Chou, Micah S. Glaz,[†] David A. Vanden Bout, and Keith J. Stevenson*

Department of Chemistry, The University of Texas at Austin, 1 University Station, Austin, Texas, 78712, United States. [†]Present address: Department of Chemistry, University of Washington, Seattle, Washington 98195, United States.

ABSTRACT An elegant method for the electrodeposition of MoS_2 thin films using room temperature ionic liquids (RTIL) as an electrolyte was developed. Simple molecular precursors of Mo and S were added in different concentrations to tune the composition and deposition process. The electrodeposition of MoS_2 was confirmed with both Raman spectroscopy and XPS. Analysis showed that the electrodeposited MoS_2 films form a flower shape morphology with edge active sites that promote the hydrogen evolution reaction (HER). Furthermore, this technique enables selective tuning of the film thickness and demonstrates high photoluminescence activity with a decrease in the number of layers.

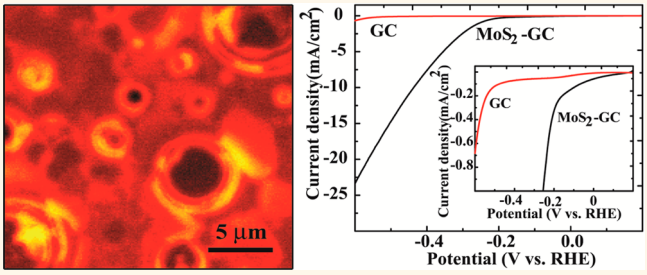

KEYWORDS: MoS_2 · electrodeposition · ionic liquid · hydrogen evolution reaction · photoluminescence

Recently, great interest has arisen toward the development of 1D and 2D materials for electronic applications. MoS_2 has been shown to outperform graphene and the other currently used silicon-based materials for electronics and energy harvesting.[1−6] The photoexcitation dynamics for the monolayer and few-layer structures were found to be remarkably different from those of thick crystals due to faster intraband relaxation rate and defect assisted scattering.[5] Thin-layered MoS_2 demonstrates enhanced electron transfer and interesting layer-dependent optical properties that could be especially useful for photoluminescence and electronic applications.[5,6] MoS_2 has also been used in replacing ubiquitous Pt electrocatalysts for the hydrogen evolution reaction (HER), where the reaction mechanism is believed to mimic the biological photosynthesis system involving the active site/cofactor nitrogenase and hydrogenase.[7] Recent computational and experimental results have confirmed the catalytic behavior of MoS_2 by elucidating the hydrogen evolution mechanism where hydrogen evolution occurs at the sulfur edges of MoS_2 planes while their basal planes remain catalytically inert.[7] There have been many attempts to improve the catalytic activity of MoS_2 films by synthesizing materials in specific orientations to increase the number of edge planes.[8−11]

Yet current synthesis methods for MoS_2 involve high temperature, high pressure, low oxygen, and other extreme conditions. They also result in the production of impure MoS_2 often intermixed with substoichiometric molybdenum oxide phases. Composites of MoS_2 have been made with carbon materials such as carbon nanotubes, graphene oxide and graphene in effort to expose the MoS_2 edge sites. This hybrid configuration showed superior electrocatalytic activity in the HER relative to other MoS_2 single crystal catalysts.[12−14] Efforts were made to manipulate the crystallinity and morphology of more active MoS_2 by adopting thermal decomposition of $(NH_4)_2MoS_4$ with different ionic liquids as solvent.[12,15] MoS_2 deposited over metal surfaces exhibit partial Fermi level pinning, thus altering the chemical reactivity of the MoS_2. This configuration apparently enhances the binding of hydrogen by as

* Address correspondence to stevenson@mail.utexas.edu.

Received for review July 17, 2013 and accepted August 20, 2013.

Published online August 20, 2013
10.1021/nn4036624

much as ~0.4 eV as a result of stronger H−S coupling enabled by charge transfer from the substrate to the MoS_2.[16] However, all these methods use presynthesized MoS_2 and involve harsh chemical pretreatments (H_2S gas) with required energy-intensive steps to produce high quality phase pure MoS_2 thin films. Other alternative techniques need to be explored to synthesize high quality MoS_2 thin films in more scalable and benign manners. An electrodeposition technique would be appropriate; nevertheless, there have been very few attempts toward the development of such procedures. Current aqueous- and nonaqueous-based cathodic electrodeposition processes use sodium tertathiomolybdate but result in either amorphous MoS_x or amorphous MoS_3 films with oxide contamination.[17−21] Postdeposition heat treatment or sulfurization is typically required to achieve the appropriate stoichiometry of Mo and S. Recently, Merki *et al.* developed an aqueous-based electropolymerization process to synthesize molybdenum sulfide for applications such as hydrogen evolution catalysis. However, the electrodeposited films were mainly amorphous and phase impure with a combination of MoS_2 and MoS_3.[22,23]

In this study, we report for the first time a nonaqueous-based electrodeposition method to produce films of stoichiometric MoS_2 using room temperature ionic liquids (RTILs) as an electrolyte with simple Mo and S precursors. RTILs offer a unique electrolyte for the electrochemical reduction of reactive metals such as Si, Ge, and Sn due to their wide electrochemical window, negligible vapor pressure, and high ionic conductivity.[24,25] Earlier, we had shown that it is possible to electrodeposit stoichiometric GeS_2 at room temperature using a RTIL.[26] Here, we used PP_{13}-TFSI (*N*-methyl-*N*-propylpiperidinium (PP_{13}) cation and bis(trifluoromethanesulfonyl)imide (TFSI) anion) as the RTIL[27] electrolyte for the electrochemical deposition of MoS_2 utilizing molybdenum glycolate and 1,4-butanedithiol as the Mo and S precursors, respectively (see Experimental Methods).

RESULTS AND DISCUSSION

Figure 1A shows the potentiodynamic deposition of MoS_2 films on a glassy carbon (GC) electrode at various temperatures. Two irreversible diffusion-controlled reduction peaks are observed at −0.75 and −1.65 V, corresponding to the reduction of Mo(VI) to Mo(V) and reduction of Mo(V) to Mo(IV), respectively. When the potential is scanned to more negative potentials than −1.65 V, the reduction of MoS_x complex takes place. This reduction requires a high overpotential. The deposition process changes with temperature and potential as suggested by the change in voltammetric response. Molybdenum glycolate has a tendency to absorb moisture in the presence of water and promote the oxidation of Mo. However, by increasing the

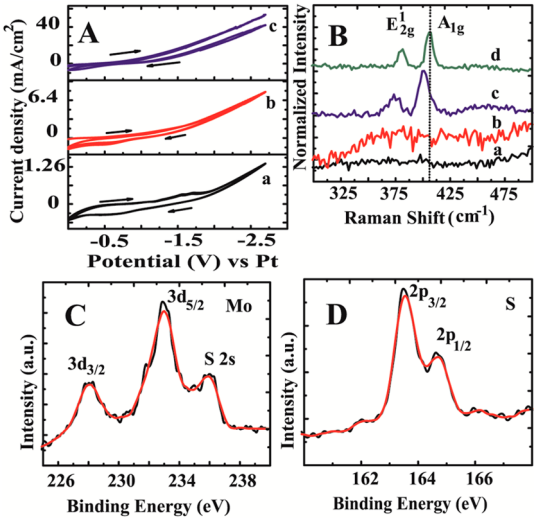

Figure 1. (A) Potentiodynamic deposition of MoS_2 film over polished GC electrodes at different temperatures (a, room temperature (rt); b, 50 °C; and c, 100 °C) with 100 μL of 1,4-butanedithiol and 100 μL of molybdenum glycolate in 1 mL of PP_{13}TFSI ionic liquid. Cycled between 0 to −2.7 V *vs* Pt (QRE) at scan rate of 100 mV/s. (B) Raman spectrum of electrodeposited MoS_2 at different temperatures. a, rt; b, 50; c, 100 °C; and d, commercial bulk MoS_2 for comparison. (C) Mo 3d XPS analysis of electrodeposited MoS_x films at 100 °C. (D) S 2p XPS analysis of MoS_2.

temperature to 100 °C, the redox peaks associated with molybdenum ions disappear. Reduction at potentials negative of −2 V leads to the direct deposition of MoS_2.[26] The electrodeposited films at various temperatures were further characterized by Raman spectroscopy (Figure 1B) to access crystallinity. The films electrodeposited at room temperature showed no distinct peaks and suggest that the films are amorphous on the GC electrode. With an increase in temperature, the Raman spectrum changes significantly. At 100 °C distinct Raman peaks start to appear at 385 and 404 cm^{-1}, corresponding to the E^1_{2g} and A_{1g} vibrational modes of crystalline MoS_2, respectively.[28] E^1_{2g} indicates planar vibration and A_{1g} is associated with the vibration of sulfides in the out-of-plane direction. The Raman shift in the peaks compared to bulk MoS_2 samples may be due the existence of only a few layer thickness film of MoS_2. This phenomenon has been reported for exfoliated layers MoS_2.[4,29,30]

MoS_2 formation was further examined and quantified by XPS analysis. The electrodeposited MoS_x films displayed the Mo $3d_{5/2}$ peak at 232.5 eV (Figure 1C), which suggests a shift of 4 eV from the expected 228.55 eV due to charging effects on the top 10 nm layer of the deposited thin film using a 1:1 Mo:S precursor ratio. Sputtering analysis of the films yielded a peak at 228 eV corresponding to the expected 228.5 eV for Mo(IV). S 2p XPS analysis showed a peak for $2p_{3/2}$ at 162.5 eV (Figure 1D), which confirms the formation of MoS_2.[31,32] Quantitative elemental analysis from high resolution XPS peak integration shows 32.94% Mo and 67.06% S, which confirmed deposition

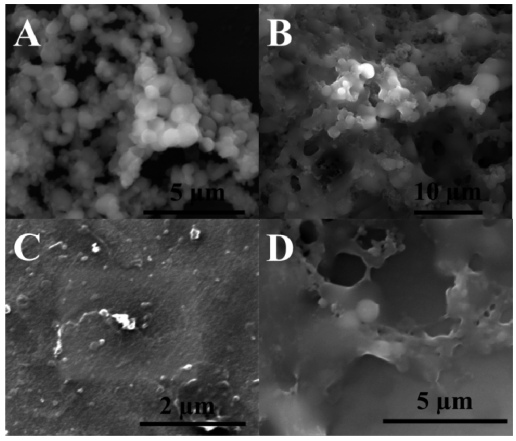

Figure 2. SEM images of potentiodynamically electrodeposited MoS_2 at various temperatures. (A) rt, (B) 50, (C) 75, and (D) 100 °C.

of MoS_2. To understand the mechanism of MoS_2 formation, depositions were performed as a function of temperature from rt to 100 °C. Figure 2 shows the SEM analysis of MoS_x depositions at various temperatures. Room-temperature deposition leads to the formation of nanoparticles of amorphous MoS_x, which is supported by Raman (Figure 1Ba) analysis showing no distinct peaks. EDS analysis confirms these particles constitute Mo and S (Figure S1, Supporting Information). With an increase in temperature, the nanoparticles of MoS_x agglomerate and fuse together to form big clusters of MoS_x (Figure 2B). Furthermore, with an increase in temperature at 75 and 100 °C (Figure 2 C,D), these fused particles form thin and smooth porous films of MoS_x. The presence of a uniform layer suggests that a layered deposition *via* sulfur complexation is analogous to the growth of larger particles *via* Oswald ripening, wherein smaller crystalline particles coalesce and form larger particles in a solvent mediated medium.[26,33] These porous smooth films were characterized as MoS_2 through Raman, XPS, and SEM-EDS analysis.

Different concentrations of S precursor were added to Mo precursor in 1:1, 1:2, and 1:3 ratios, and depositions were performed at 100 °C potentiodynamically from 0 to −2.7 V *vs* Pt (QRE). Raman analysis of electrodeposited samples confirms that the increase in concentration produces extra sulfur peak around 310 cm^{-1}, and this peak grows with an increase in concentration (Figure S2, Supporting Information). Only 1:1 ratio of S and Mo precursors forms stoichiometric MoS_2 without any impurities. To understand the MoS_2 formation at 100 °C, chronoamperometric depositions were performed at various reduction potentials (−1.5, −2, and −2.7 V *vs* Pt). Deposition at −2.7 V shows the irregularity in the *i*−*t* curve confirming the growth of MoS_2 (Figure S3, Supporting Information). This irregular current response may be due to the complex nature of the process involving heterogeneous nucleation of MoS_2 from the ionic

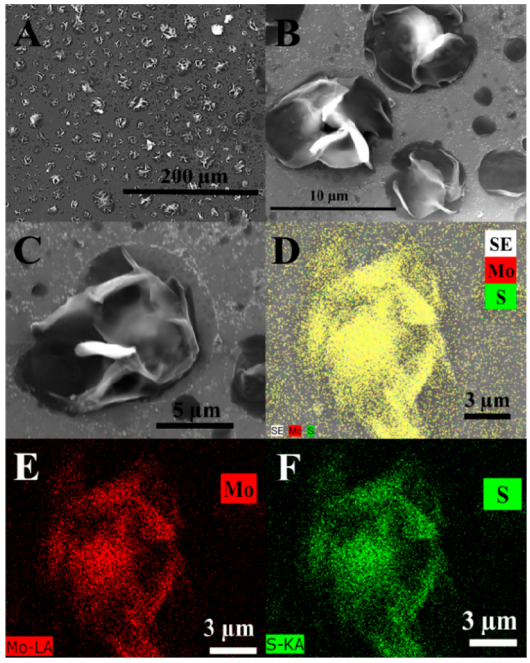

Figure 3. (A) SEM-EDS analysis of chronoamperometrically at −2.7 V *vs* Pt electrodeposited MoS_2 over glassy carbon electrodes showing the formation of flower morphology. (B,C) Enlarged and closer view of MoS_2 flower morphology. (D) Elemental analysis of MoS_2 showing the presence of Mo and S in the secondary electron (SE) image. (E) Elemental analysis of showing the presence of Mo. (F) Elemental analysis showing the presence of S.

liquid mediated complex and also influenced by a resistive contact with the GC substrate.[26,34] However, use of metal surfaces for the deposition can show different behavior. Metals exhibit partial Fermi level pinning with MoS_2 and results in a strong interaction.[16] The growth of MoS_2 takes place after the potential −2 V *vs* Pt confirmed by the Raman spectrum (Figure S4, Supporting Information). The peaks at 380 and 405 cm^{-1} grow with an increase in potential and −2.7 V *vs* Pt sharp peaks were obtained, confirming the formation of crystalline MoS_2. Figure 3 shows the MoS_2 film deposited on GC at −2.7 V *vs* Pt (QRE) at 100 °C. The SEM images show that the film is quite uniform with a distinct flower-like morphology (Figure 3A), and the enlarged image shows that the surface contains small spherical flower-like particles (Figure 3B,C). The agglomeration of MoS_x particles continued into a layered flower-like morphology of up to 2 μm, which are confirmed to be MoS_x by EDS analysis (Figure 3 D−F). This agrees well with the formation and growth mechanism of metal chalcogenides with the complexation of ionic liquid precursors. Presumably, the loss of moisture in the Mo precursor by heating at 100 °C helps the reaction of S precursors. This is further supported by CVs at 100 °C, which show the loss of oxidation peaks as compared to the rt and 50 °C depositions that show predominant peaks at −1.25 and 0.65 V. The flower-like morphology promotes more edge sites compared to a uniform film. These edge sites are

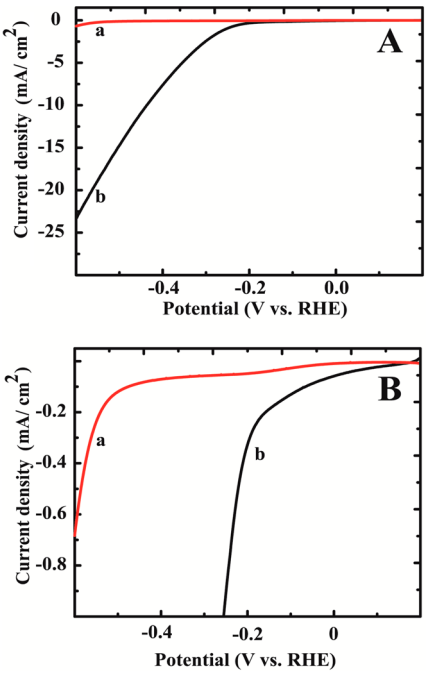

Figure 4. (A) Hydrogen evolution reaction (HER) in 0.5 M H_2SO_4 at the scan rate of 2 mV/s at GC (a) and at MoS_2 electrodeposited over GC (b). (B) Onset potential of GC (a) and MoS_2 over GC electrode (b).

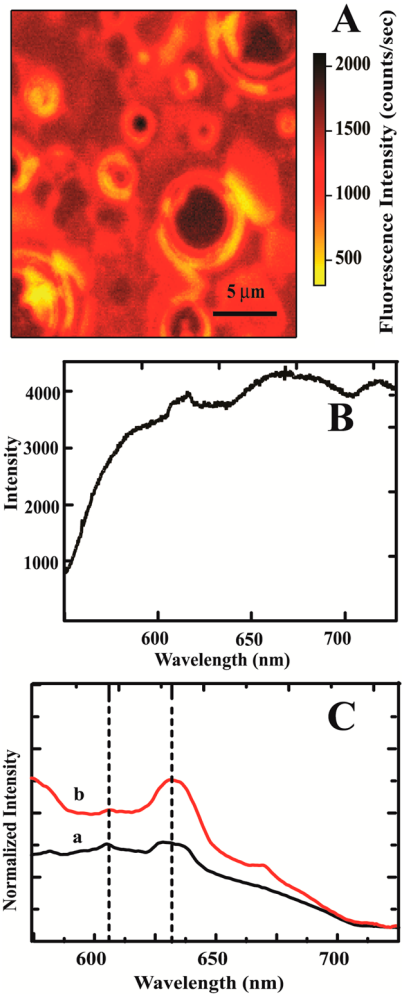

Figure 5. (A) Fluorescence scanning confocal optical microscopy image of electrodeposited MoS_2 at 100 °C on GC electrodes. (B) Accumulated spectra collected in the region of fluorescence imaging. (C) Bulk fluorescence spectrum collected over the large area exposed sample in a right angle mode for electrodeposited MoS_2 for 600 s (a) and 300 s (b) at −2.7 V *vs* Pt (QRE).

essential for the hydrogen evolution reaction as it mimics electronically and structurally biologically formed nitrogenase enzyme. Usually this MoS_2 flower morphology has been found to form at high temperature (1000 °C) during sulfurization of MoO_2.[35] Our synthesis method has shown that these active sites can be obtained by an electrodeposition process. This kind of flower-like morphology has also been reported by chemical vapor deposition growth of metal chalcogenides through boundary layer diffusion mediated process such as GeS.[36]

To evaluate the catalytic activity of electrodeposited MoS_2 over GC, the HER was examined in 0.5 M H_2SO_4. Linear sweep voltammetry (LSV) was used to determine the kinetic activity of the deposited films. Figure 4A shows the results of LSVs compared to those conducted on bare GC to find the reduction overpotential for hydrogen evolution. From the polarization measurements, maximum current density of 22 mA/cm^2 was obtained at −0.6 V *vs* RHE. These MoS_2 films display an onset potential for hydrogen evolution with high catalytic current densities of 0.18 and 0.34 mA/cm^2 at $\eta = 100$ and 200 mV, respectively (Figure 4B). This onset potential for HER is similar to the MoS_2 reported in the literature.[9,22,37] The polarization curves remain stable even after 25 scans confirming the electrodeposited MoS_2 are stable as HER catalysts (Figure S5, Supporting Information). A Tafel analysis was conducted on the polarization curves to determine the catalytic activity of the electrochemical reduction process. The overpotential η (V) observed during an experiment is given by $\eta = a + b \ln j$ where a (V) is the Tafel constant, b (V dec^{-1}) is the Tafel slope and j (mA cm^{-2}) is the current density. The Tafel slope is an inherent property of the catalyst determined by the rate limiting step of the HER reaction (Figure S6, Supporting Information). The linear portions of the Tafel curve were fit to the Tafel equation at the point of hydrogen evolution. The Tafel response was then determined to be 106 mV/decade corresponding to the slope of the linear response region. The low overpotential region shows a different Tafel slope, which is possibly due to the potential dependent surface coverage of hydrogen and reflects a change in the activation barrier. Presumably, the flower morphology increases the number of catalytically active edge sites for enhanced hydrogen evolution. H_2 evolution by MoS_2 with the flower-like morphology appears to proceed *via* a different mechanism than that observed at single crystal or nanoparticulate MoS_2. This Tafel slope is different from those of MoS_2 crystals (55−60 mV per decade) or MoS_2 nanoparticles

(120 mV per decade). This difference in the Tafel slope reported for MoS_2 from 40 to 120 mV/decade is a result of the variation of the synthesis conditions.[16,37] Some theoretical studies have been performed to understand the mechanism of HER in MoS_2.[38] This study suggests that the values obtained in this work are in close agreement with the theoretical slope of 120 mV/decade in which adsorption of protons at MoS_2 is the rate-limiting step.[39,40]

Ultrathin layers of MoS_2 are also known to exhibit photoluminescence properties. In order to interrogate the photoluminescence behavior of the electrodeposited MoS_2 films, we employed a scanning confocal microscope coupled with a spectrometer (see Experimental Methods). The electrodeposited MoS_2 over GC sample showed fluorescence behavior when excited at 488 nm, (Figure 5A) suggesting that the electrodeposited films are of few layer thickness. The edge sites in the electrodeposited samples showed higher fluorescence intensity. The averaged spectrum obtained from the image shows distinct peaks at 615 and 675 nm (Figure 5B) further confirming the photoluminescence aspect of MoS_2 in electrodeposited films. Furthermore, the thickness of the films were varied by the electrodeposition time at a constant potential (−2.7 V *vs* Pt (QRE)) for 300 and 600 s. Figure 5C shows that the bulk photoluminescence increases in the intensity at 615 and 675 nm for thinner films deposited for 300 s compared to those for 600 s. Collectively, the fluorescence and Raman spectra indicate that an ultrathin single layer was deposited. In particular, the Raman peak at 385 cm^{-1} corresponds to the E^1_{2g} vibrational mode, while the peak 403 cm^{-1} corresponds directly with the A_{1g} mode. As reported elsewhere, the E^1_{2g} mode softens and A_{1g} mode broadens with an increase in the number of layers.[4,29,30] This characteristic shift of the A_{1g} mode suggests the deposition of an ultrathin layer that displays fluorescent properties.

CONCLUSIONS

In summary, a facile electrochemical method for the deposition of MoS_2 films using ionic liquids has been demonstrated. This synthesis technique is especially useful for low cost, environmentally friendly synthesis of molybdenum chalcogenides and mixed metal chalcogenides. Creation of flower-like morphology leads to formation of active edge sites. The hydrogen evolution reaction with the electrodeposited MoS_2 films yielded 106 mV/decade Tafel slope suggesting that the rate determining step is adsorption of protons on the catalyst surface. Electrodeposited few-layer MoS_2 showed characteristic fluorescent properties demonstrating that these materials have the optoelectronic properties of ultrathin film MoS_2 desired for applications such as photodetectors and light emitting devices.

EXPERIMENTAL METHODS

The PP_{13}-TFSI room temperature ionic liquid (RTIL) was synthesized *via* a published procedure.[26,27] Molybdenum glycolate was used as the Mo precursor; it is prepared by refluxing 1.5 g MoO_3 (Sigma-Aldrich, 99.95% Reagent Plus) with 250 mL of ethylene glycol (Fisher Scientific, laboratory grade) at 194 °C for 1 h under N_2 atm. Brown color viscous final product was extracted after the reaction.[41,42]

The MoS_2 films were deposited from a molybdenum source and a sulfur source mixed in 1:1 volume ratio. A home-built electrochemical cell was used to deposit the MoS_2 film on glassy carbon (GC) substrates (Alfa Aesar, 1 mm thick, Type 2). GC substrates were used as the working electrode. The GC substrates were polished with 0.05 μm alumina slurry on microcloth (Buehler) and sonicated in 18.2 MΩ cm water prior to the deposition. Pt was used as a counter electrode and a quasireference electrode (QRE). Potentiodynamic depositions were performed at the scan rate of 100 mV/s for different temperatures (rt, 50, 75, and 100 °C). The chronoamperometric deposition was conducted under varying potentials (−2.7, −2.5, −2, −1.5, and −1 V) at a constant temperature of 100 °C. The cell was placed in a sand-bath on a hot plate (Thermolyne Nuova II stir plate). Additional experiments were carried out at a constant potential of −2.7 V by varying the temperature (25, 50, 60, 70, 80, 90 °C) using chronoamperometric deposition. The synthesized MoS_x films were washed with acetone and stored in a desiccator. All electrochemical experiments were performed with a CH Instruments Electrochemical Workstation CHI 440. Electrochemical studies of the hydrogen evolution reaction (HER) were conducted using a three cell assembly in 0.5 M H_2SO_4 electrolyte.[22] MoS_2 films deposited over GC were used as the working electrode. All the depositions were performed with GC (1 × 1 cm) piece. GC piece was mounted on a GC (PINE Instruments AFE2M050GC) rotating disc electrode surface with double sided carbon tape (Ted Pella). The active area of the electrodes was 0.36 cm^2. Pt was used as a counter electrode, and Ag/AgCl (KCl saturated) as the reference electrode. Potentials were referenced to reversible hydrogen electrode (RHE) by adding a value of (0.197 + 0.059 pH) V. Both cyclic voltammetry (CV) and linear sweep voltammetry (LSV) techniques were conducted under scan rate of 100 and 2 mV/s, respectively, on the three electrode setup at potentials of 0 to −0.8 V *vs* Ag/AgCl. Tafel analysis was carried out by plotting V *vs* log I from the LSV curve to determine the slope of the log plot. The Tafel slope was used to determine the kinetic activity of the electrode.[7] The slopes are evaluated in the low overpotential region to avoid the contribution of ohmic resistance to the Tafel slope.[37]

Raman spectroscopy was performed with a Renishaw In Via microscope system utilizing a 514.5 nm Ar laser in backscattering configuration. The instrument was calibrated to the Stokes Raman signal at 521 cm^{-1} using a bulk single crystal of Si with the direction oriented normal to the laser. A 50× aperture was used, resulting in an approximately 2 μm diameter sampling cross section. The spectral samples were collected over 20 s exposure time. The Raman peaks were used to determine the two modes of deposition of MoS_2. The 385 cm^{-1} peak would correspond to the E^1_{2g} vibrational mode, and the 404 cm^{-1} peak corresponds directly with the A_{1g} mode. E^1_{2g} indicates planar vibration and A_{1g} associated with the vibration of sulfides in the out-of-plane direction. The Raman characterization was carried out on each of the deposited GC substrates.

X-ray photoelectron spectroscopy (XPS) was used to analyze the chemical environment of elements present in MoS_x. XPS was carried out with a Kratos AXIS Ultra DLD system calibrated using the signals for Au $4f_{7/2}$ at 83.98 eV. Spectra were collected at 0.05 eV steps with 1000 ms integration time at each step, and the measurements were conducted under a vacuum of

10^{-9} Torr. Sputtering experiments were conducted at 4 kV. XPS samples were prepared by constant potential deposition at −2.7 V at 100 °C.

Scanning electron microscopy (SEM) was performed with a Quanta 650 operated at 30.00 kV. Electrodeposited MoS_x films over GC (1 cm × 1 cm) were mounted on the Al stub with double sided carbon tape (Ted Pella) for the SEM analysis. SEM was used to determine the morphology of the deposited film on GC substrates at varying potentials. EDS analysis was performed to determine the relative ratios of Mo/S on the deposited thin films.

Scanning confocal measurements were obtained using the 488 nm line of an argon Ion laser. The beam was focused using a 50× Olympus objective, and the sample was rastered scanned across the beam using a Physik Instrumente (PI) piezoelectric stage, which was mounted onto a Nikon Diaphot 300 inverted microscope. The fluorescence was collected using a Perkin-Elmer APD, and spectra were collected using an Acton spectrometer attached to a liquid-nitrogen-cooled charged coupled device (LN-CCD) from Princeton Instruments.

Conflict of Interest: The authors declare no competing financial interest.

Supporting Information Available: SEM-EDS analysis of electrodeposited MoS films; *i*−*t* behavior of electrodeposition process and Raman analysis; Tafel plot analysis of hydrogen evolution reaction. This material is available free of charge *via* the Internet at http://pubs.acs.org.

Acknowledgment. Financial support of this work was provided by the R.A. Welch Foundation (Grant F-1529). We thank Jake Goran and Matthew Charlton for assistance with the XPS measurements. The Kratos XPS was funded by the National Science Foundation under Grant CHE-0618242. M.S.G. would like to acknowledge the NSF IGERT program (DGE-054917) for financial support.

REFERENCES AND NOTES

1. Butler, S. Z.; Hollen, S. M.; Cao, L.; Cui, Y.; Gupta, J. A.; Gutiérrez, H. R.; Heinz, T. F.; Hong, S. S.; Huang, J.; Ismach, A. F.; et al. Progress, Challenges, and Opportunities in Two-Dimensional Materials Beyond Graphene. *ACS Nano* **2013**, *7*, 2898–2926.
2. Yoon, Y.; Ganapathi, K.; Salahuddin, S. How Good Can Monolayer MoS_2 Transistors Be?. *Nano Lett.* **2011**, *11*, 3768–3773.
3. Radisavljevic, B.; Radenovic, A.; Brivio, J.; Giacometti, V.; Kis, A. Single-Layer MoS_2 transistors. *Nat. Nanotechnol.* **2011**, *6*, 147–150.
4. Lee, C.; Yan, H.; Brus, L. E.; Heinz, T. F.; Hone, J.; Ryu, S. Anomalous Lattice Vibrations of Single and Few-Layer MoS_2. *ACS Nano* **2010**, *4*, 2695–2700.
5. Eda, G.; Yamaguchi, H.; Voiry, D.; Fujita, T.; Chen, M.; Chhowalla, M. Photoluminescence from Chemically Exfoliated MoS_2. *Nano Lett.* **2011**, *11*, 5111–5116.
6. Splendiani, A.; Sun, L.; Zhang, Y.; Li, T.; Kim, J.; Chim, C.-Y.; Galli, G.; Wang, F. Emerging Photoluminescence in Monolayer MoS_2. *Nano Lett.* **2010**, *10*, 1271–1275.
7. Hinnemann, B.; Moses, P. G.; Bonde, J.; Jørgensen, K. P.; Nielsen, J. H.; Horch, S.; Chorkendorff, I.; Nørskov, J. K. Biomimetic Hydrogen Evolution: MoS_2 Nanoparticles as Catalyst for Hydrogen Evolution. *J. Am. Chem. Soc.* **2005**, *127*, 5308–5309.
8. Kibsgaard, J.; Chen, Z.; Reinecke, B. N.; Jaramillo, T. F. Engineering the Surface Structure of MoS_2 to Preferentially Expose Active Edge Sites for Electrocatalysis. *Nat. Mater.* **2012**, *11*, 963–969.
9. Jaramillo, T. F.; Jørgensen, K. P.; Bonde, J.; Nielsen, J. H.; Horch, S.; Chorkendorff, I. Identification of Active Edge Sites for Electrochemical H_2 Evolution from MoS_2 Nanocatalysts. *Science* **2007**, *317*, 100–102.
10. Karunadasa, H. I.; Montalvo, E.; Sun, Y.; Majda, M.; Long, J. R.; Chang, C. J. A Molecular MoS_2 Edge Site Mimic for Catalytic Hydrogen Generation. *Science* **2012**, *335*, 698–702.
11. Kong, D.; Wang, H.; Cha, J. J.; Pasta, M.; Koski, K. J.; Yao, J.; Cui, Y. Synthesis of MoS_2 and $MoSe_2$ Films with Vertically Aligned Layers. *Nano Lett.* **2013**, *13*, 1341–1347.
12. Lau, V. W.-h.; Masters, A. F.; Bond, A. M.; Maschmeyer, T. Promoting the Formation of Active Sites with Ionic Liquids: A Case Study of MoS_2 as Hydrogen-Evolution-Reaction Electrocatalyst. *ChemCatChem* **2011**, *3*, 1739–1742.
13. Vrubel, H.; Merki, D.; Hu, X. Hydrogen Evolution Catalyzed by MoS_3 and MoS_2 Particles. *Energy Environ. Sci.* **2012**, *5*, 6136–6144.
14. Yan, Y.; Xia, B.; Qi, X.; Wang, H.; Xu, R.; Wang, J.-Y.; Zhang, H.; Wang, X. Nano-Tungsten Carbide Decorated Graphene as Co-Catalysts for Enhanced Hydrogen Evolution on Molybdenum Disulfide. *Chem. Commun.* **2013**, *49*, 4884–4886.
15. Lau, V. W.-h.; Masters, A. F.; Bond, A. M.; Maschmeyer, T. Ionic-Liquid-Mediated Active-Site Control of MoS_2 for the Electrocatalytic Hydrogen Evolution Reaction. *Chem.—Eur. J.* **2012**, *18*, 8230–8239.
16. Chen, Z.; Cummins, D.; Reinecke, B. N.; Clark, E.; Sunkara, M. K.; Jaramillo, T. F. Core−Shell MoO_3−MoS_2 Nanowires for Hydrogen Evolution: A Functional Design for Electrocatalytic Materials. *Nano Lett.* **2011**, *11*, 4168–4175.
17. Ponomarev, E. A.; Neumann-Spallart, M.; Hodes, G.; Lévy-Clément, C. Electrochemical Deposition of MoS_2 Thin Films by Reduction of Tetrathiomolybdate. *Thin Solid Films* **1996**, *280*, 86–89.
18. Bhattacharya, R. N.; Lee, C. Y.; Pollak, F. H.; Schleich, D. M. Optical Study of Amorphous MoS_3: Determination of the Fundamental Energy Gap. *J. Non-Cryst. Solids* **1987**, *91*, 235–242.
19. Albu-Yaron, A.; Lévy-Clément, C.; Katty, A.; Bastide, S.; Tenne, R. Influence of the Electrochemical Deposition Parameters on the Microstructure of MoS_2 Thin Films. *Thin Solid Films* **2000**, *361*−*362*, 223–228.
20. Hahn, B. P.; Stevenson, K. J. Cathodic Electrodeposition of Mixed Molybdenum−Selenium Oxides. *J. Electroanal. Chem.* **2010**, *638*, 151–160.
21. Albu-Yaron, A.; Levy-Clement, C.; Hutchison, J. L. A Study on MoS_2 Thin Films Electrochemically Deposited in Ethylene Glycol at 165°C. *Electrochem. Solid-State Lett.* **1999**, *2*, 627–630.
22. Merki, D.; Fierro, S.; Vrubel, H.; Hu, X. Amorphous Molybdenum Sulfide Films as Catalysts for Electrochemical Hydrogen Production in Water. *Chem. Sci.* **2011**, *2*, 1262–1267.
23. Merki, D.; Hu, X. Recent Developments of Molybdenum and Tungsten Sulfides as Hydrogen Evolution Catalysts. *Energy Environ. Sci.* **2011**, *4*, 3878–3888.
24. Al-Salman, R.; Meng, X.; Zhao, J.; Li, Y.; Kynast, U.; Lezhnina, M. M.; Endres, F. Semiconductor Nanostructures *via* Electrodeposition from Ionic Liquids. *Pure Appl. Chem.* **2010**, *82*, 1673–1698.
25. Ohno, H.; Yoshizawa, M.; Mizumo, T. Ionic Conductivity. In *Electrochemical Aspects of Ionic Liquids*; John Wiley & Sons, Inc.: Hoboken, New Jersey, 2005; pp 75−81.
26. Murugesan, S.; Kearns, P.; Stevenson, K. J. Electrochemical Deposition of Germanium Sulfide from Room-Temperature Ionic Liquids and Subsequent Ag Doping in an Aqueous Solution. *Langmuir* **2012**, *28*, 5513–5517.
27. Sakaebe, H.; Matsumoto, H. N-Methyl-N-propylpiperidinium bis(trifluoromethanesulfonyl)imide (PP_{13}-TFSI)—Novel Electrolyte Base for Li Battery. *Electrochem. Commun.* **2003**, *5*, 594–598.
28. Frey, G. L.; Tenne, R.; Matthews, M. J.; Dresselhaus, M. S.; Dresselhaus, G. Raman and Resonance Raman Investigation of MoS_2 Nanoparticles. *Phys. Rev. B: Condens. Matter Mater. Phys.* **1999**, *60*, 2883–2892.
29. Chakraborty, B.; Matte, H. S. S. R.; Sood, A. K.; Rao, C. N. R. Layer-Dependent Resonant Raman Scattering of a Few Layer MoS_2. *J. Raman Spectrosc.* **2013**, *44*, 92–96.
30. Molina-Sánchez, A.; Wirtz, L. Phonons in Single-Layer and Few-Layer MoS_2 and WS_2. *Phys. Rev. B: Condens. Matter Mater. Phys.* **2011**, *84*, 155413.

31. Wang, X.; Feng, H.; Wu, Y.; Jiao, L. Controlled Synthesis of Highly Crystalline MoS_2 Flakes by Chemical Vapor Deposition. *J. Am. Chem. Soc.* **2013**, *135*, 5304–5307.
32. Patterson, T. A.; Carver, J. C.; Leyden, D. E.; Hercules, D. M. A surface Study of Cobalt-Molybdena-Alumina Catalysts using X-ray Photoelectron Spectroscopy. *J. Phys. Chem.* **1976**, *80*, 1700–1708.
33. Freyland, W.; Aravinda, C. L.; Borissov, D. Nanoscale Electrocrystallization of Metals and Semiconductors from Ionic Liquids. In *Electrocrystallization in Nanotechnology*; Wiley-VCH Verlag GmbH & Co. KGaA: Weinheim, 2007; pp 79−95.
34. Tributsch, H.; Bennett, J. C. Electrochemistry and Photochemistry of MoS_2 Layer Crystals. I. *J. Electroanal. Chem. Interfacial Electrochem.* **1977**, *81*, 97–111.
35. Li, Y. B.; Bando, Y.; Golberg, D. MoS_2 Nanoflowers and their Field-Emission Properties. *Appl. Phys. Lett.* **2003**, *82*, 1962–1964.
36. Li, C.; Huang, L.; Snigdha, G. P.; Yu, Y.; Cao, L. Role of Boundary Layer Diffusion in Vapor Deposition Growth of Chalcogenide Nanosheets: The Case of GeS. *ACS Nano* **2012**, *6*, 8868–8877.
37. Laursen, A. B.; Kegnaes, S.; Dahl, S.; Chorkendorff, I. Molybdenum Sulfides—Efficient and Viable Materials for Electro- and Photoelectrocatalytic Hydrogen Evolution. *Energy Environ. Sci.* **2012**, *5*, 5577–5591.
38. Skúlason, E.; Tripkovic, V.; Björketun, M. E.; Gudmundsdóttir, S. d.; Karlberg, G.; Rossmeisl, J.; Bligaard, T.; Jónsson, H.; Nørskov, J. K. Modeling the Electrochemical Hydrogen Oxidation and Evolution Reactions on the Basis of Density Functional Theory Calculations. *J. Phys. Chem. C* **2010**, *114*, 18182–18197.
39. Appleby, A.; Zagal, J. Free Energy Relationships in Electrochemistry: A History that Started in 1935. *J. Solid State Electrochem.* **2011**, *15*, 1811–1832.
40. Fletcher, S. Tafel Slopes from First Principles. *J. Solid State Electrochem.* **2009**, *13*, 537–549.
41. Cuin, A.; Massabni, A. C. Synthesis and Characterization of Solid Molybdenum(VI) Complexes with Glycolic, Mandelic and Tartaric acids. Photochemistry Behaviour of the Glycolate Molybdenum Complex. *J. Coord. Chem.* **2007**, *60*, 1933–1940.
42. Preiss, H.; Meyer, B.; Olschewski, C. Preparation of Molybdenum and Tungsten Carbides from Solution Derived Precursors. *J. Mater. Sci.* **1998**, *33*, 713–722.